Inorganic Chemistry

Article

pubs.acs.org/IC

Interplay of Octahedral Rotations and Lone Pair Ferroelectricity in $CsPbF_3$

Eva H. Smith,[*,†] Nicole A. Benedek,[*,‡,§] and Craig J. Fennie[†]

[†]School of Applied and Engineering Physics, Cornell University, Ithaca, New York 14853, United States

[‡]Materials Science and Engineering Program, University of Texas at Austin, 1 University Station, Austin, Texas 78712, United States

[§]Department of Materials Science and Engineering, Cornell University, Ithaca, New York 14853, United States

Supporting Information

ABSTRACT: $CsPbF_3$ is the only experimentally synthesized ABF_3 fluoride perovskite with a polar ground state. We use $CsPbF_3$ as a guide in our search for rules to rationally design new ABX_3 polar fluorides and halides from first-principles and as a model compound to study the interactions of lone pairs, octahedral rotations, and A- and B-site driven ferroelectricity. We find that the lone pair cation on the B-site serves to stabilize a polar ground state, analogous to the role of lone pair cations on the A-site of oxide perovskites. However, we also find that the lone pair determines the pattern of nonpolar structural distortions, rotations of the PbF_6 octahedra, that characterize the lowest energy structure. This result is remarkable since rotations are typically associated with bonding preferences of the A-site cation (here Cs^+), whereas the Pb^{2+} cation occupies the B site. We show that the coordination requirements of the A-site cation and the stereoactivity of the B-site lone pair cation compete or cooperate via the anionic displacements that accompany polar distortions. We consider the generalizability of our findings for $CsPbF_3$ and how they may be extended to the oxide perovskites as well as to the organic−inorganic hybrid halide perovskite photovoltaics.

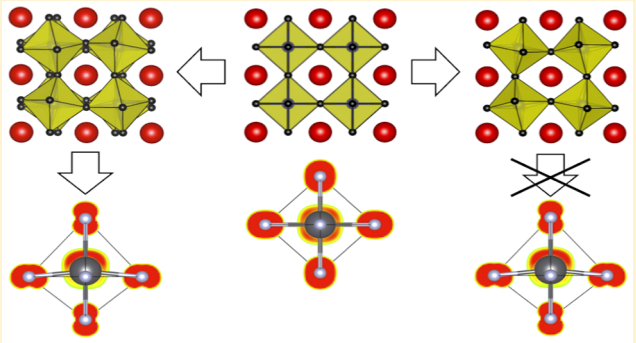

INTRODUCTION

While a great body of research has been devoted to the study of and search for design principles for polar and ferroelectric oxide perovskites, polar or ferroelectric *fluoride* perovskites have not received nearly as much attention. There are about 120 combinations of monatomic cations A^+ and B^{2+} that, if combined with F^- in the stoichiometry ABF_3, would exhibit Goldschmidt tolerance factors[1] between 0.76 and 1.13, the criterion for stability for fluoride perovskites.[2] Between the Inorganic Crystal Structure Database[3] and the Landolt−Börnstein tables,[4] we located structural reports for nearly 70 stoichiometric ABF_3 perovskites. The great majority of these reports are for experimentally synthesized structures characterized at room temperature. Computational and low-temperature reports are scarce.

$CsPbF_3$ (tolerance factor, t = 0.94) is the only ABF_3 perovskite experimentally observed to form in a polar structure and is one of few inorganic ABX_3 perovskites with a lone pair cation (Pb^{2+}) on the B-site. Rather than being merely a curiosity, on the contrary this positions $CsPbF_3$ as a bridge between the extensive inorganic (mostly oxide) perovskite literature and the rapidly growing field of hybrid organic−inorganic halide perovskite photovoltaics in which the A-site cation is a small organic molecule, the B-site cation is most often Pb^{2+} but occasionally another 2+ lone pair cation, and the anions are halides.[5−7] Because of the great technological importance of the oxide perovskites and of the hybrid perovskite photovoltaics, we use our findings for $CsPbF_3$ to shed light on both families of materials.

The low-temperature polar $R3c$ phase (space group no. 161) of $CsPbF_3$ is reached by a discontinuous transition at 186 K from the high-temperature $Pm\bar{3}m$ (space group no. 221) cubic perovskite structure.[8] The $R3c$ structure is obtained from $Pm\bar{3}m$ by a rotation of the PbF_6 octahedra about the [111] axis with respect to the cubic perovskite cell (Glazer tilt pattern[9] $a^-a^-a^-$) followed by polar displacements along the same axis. It is surprising that $CsPbF_3$ adopts a rhombohedral structure because extensive crystal chemical studies of oxides have shown that the stability of the rhombohedral distortion depends on the crystal Madelung energy[10] and therefore decreases as the charge of the A-site cation decreases. In addition, although first-principles and lattice energy calculations have shown that the Glazer tilt patterns $a^-b^+a^-$ (leading to space group $Pnma$, no. 62) and $a^-a^-a^-$ (leading to space group $R\bar{3}c$, no. 167) are energetically comparable in most perovskites, repulsive anion−anion interactions in $a^-a^-a^-$ increase as the tilting angle increases.[10,11] Given these observations, an ABF_3 perovskite with a monovalent A-site cation would not be expected to adopt a rhombohedral structure. Indeed, Berastegui

Received: May 28, 2015
Published: August 21, 2015

DOI: 10.1021/acs.inorgchem.5b01213
Inorg. Chem. 2015, 54, 8536−8543

and co-workers[8] noted that of the perovskite fluorides reported in the ICSD, none except $CsPbF_3$ are rhombohedral. The fact that $CsPbF_3$ is polar is also somewhat surprising, since the greater ionicity of the fluoride bond[2] (compared with oxides) is generally thought[12] to disfavor the acentric displacements required for ferroelectricity.

We have used first-principles calculations and simple crystal chemical models to demonstrate that the Pb^{2+} lone pair of polar fluoride perovskite $CsPbF_3$ is responsible for both the ferroelectricity and particular octahedral rotation pattern of its lowest energy structure. This result is remarkable since rotations are typically associated with bonding preferences of the A-site cation (here Cs^+), whereas the Pb^{2+} cation occupies the B-site. We demonstrate that localization of the Pb^{2+} lone pair requires significant anionic displacements, which also modify the A-site environment. Whether these modifications are favorable or unfavorable depends strongly on octahedral rotation pattern; unfavorable interactions suppress lone pair localization, while favorable interactions characterize the lowest energy structure. Our work thus demonstrates the mechanism by which cationic lone pairs may influence both polar and nonpolar structural distortions, as well as how the interplay between the chemistries of the A and B cations gives rise to the ground state.

COMPUTATIONAL METHODS

Calculations were performed using the PBEsol functional[13] as implemented in the Vienna *ab initio* simulation package (VASP),[14,15] with a plane wave cutoff of 600 eV and a 5 × 5 × 5 Γ-centered k-point mesh. Lattice dynamical properties (phonon modes and frequencies) were calculated using density functional perturbation theory,[16,17] and phonon frequencies were converged to within 5 cm^{-1} with respect to energy cutoff and k-point mesh. Relaxations were considered complete when residual forces on all atoms were less than 0.25 meV/Å. PAW potentials supplied by the VASP package[18] were used, with the following valence states: Cs, $5s^25p^66s^1$; Sr, $4s^24p^65s^2$; Pb, $5d^{10}6s^26p^2$; F, $2s^22p^5$. Tolerance factors and bond valences were calculated using Brese and O'Keeffe's bond valence parameters[19] assuming a 12-coordinate A-site cation and a 6-coordinate B-site cation unless otherwise noted. A *b* value of 0.37 was used throughout. Our crystallographic analyses were performed using the ISOTROPY package[20] and the AMPLIMODES program of the Bilbao Crystallographic Server.[21−25] Wannier90[26] was used to find the orbital-projected densities of states[27] starting from a high-accuracy electronic structure calculated with VASP. For density of states calculations, a 12 × 12 × 12 k-point mesh was used. Crystal structures were visualized using VESTA.[28] Software version information is given in the Supporting Information.

All Miller indices are with respect to the cubic perovskite cell. We use the terms "ferroelectric" and "ferroelectricity" to refer to polar structures in which the polarization could, in principle, be switched to a symmetry-equivalent state with the application of a modest electric field. When multiple settings of a space group are allowed, we give the International notation symbol corresponding to a unique *b* axis. LO−TO splitting of zone-center phonon mode frequencies is found using Phonopy.[29]

RESULTS AND DISCUSSION

Influence of the Lone Pair in the Structural Distortions and Ground State of $CsPbF_3$ Compared with $CsSrF_3$. Stereoactive cationic lone pairs drive ferroelectricity in a number of perovskite oxides (e.g., $PbTiO_3$ and $BiFeO_3$) but are not localized in others (e.g., $PbCrO_3$,[30] $BiScO_3$,[31] and $BiGaO_3$[32]). To elucidate the role of the Pb^{2+} lone pair in the ferroelectricity of $CsPbF_3$, we compare $CsPbF_3$ with $CsSrF_3$; Sr^{2+} has almost the same ionic radius as Pb^{2+} in octahedral coordination but no lone pair. Table 1 shows that

Table 1. Comparison of Phonon Modes for $CsPbF_3$ and $CsSrF_3$ in the Fully Relaxed Cubic Perovskite Structure (Space Group $Pm\bar{3}m$)[a]

irrep	$CsPbF_3$ ω, cm^{-1}	$CsSrF_3$ ω, cm^{-1}	description
Γ_4^-	*i*60, *i*58	25, 73	polar mode
Γ_5^-	*i*33	61	antipolar F motion
M_3^+	*i*76	*i*52	in-phase octahedral rotation
M_5^-	*i*45	13	antipolar Pb motion
R_4^+	*i*79	*i*58	out-of-phase octahedral rotation
X_5^-	*i*38	47	antipolar F motion

[a]Modes with imaginary frequencies indicate structural instabilities. All unstable modes for both compounds are listed. In $CsSrF_3$, the softest LO and softest TO Γ_4^- phonon frequencies are given. The two types of octahedral rotations are illustrated in Figure 1. Phonon band structures and phonon densities of states for $CsPbF_3$ and $CsSrF_3$ are given in the Supporting Information, Figure S1.

whereas $CsPbF_3$ is unstable to both polar distortions and octahedral rotations, $CsSrF_3$ is only unstable to octahedral rotations and has no polar instability, indicating that ferroelectricity in $CsPbF_3$ is driven by the Pb^{2+} lone pair. We find that the lowest energy structure of $CsSrF_3$ is *Pnma* (established by a combination of rotation distortions transforming like the irreducible representations [irreps] M_3^+ and R_4^+, bottom right corner of Figure 1), consistent with what one would expect[33] for an oxide perovskite of the same tolerance factor (0.95).

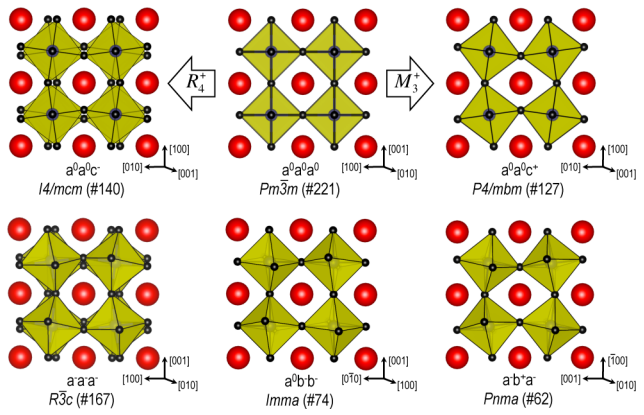

Figure 1. Illustration of "in-phase" (irrep M_3^+, top right) and "out-of-phase" (irrep R_4^+, top left) octahedral rotations about the [001] axis acting on the $Pm\bar{3}m$ aristotype (top center), as well as illustration of how rotations about multiple axes modify the structure (bottom row). Magnitudes *a*, *b*, and *c* are chosen arbitrarily for structures shown. Axes are with respect to the pseudocubic cell. A-site cations are shown as red spheres, and B-site cations sit in the centers of the yellow anion octahedra.

In contrast to $CsSrF_3$, we find that the ground state structure of $CsPbF_3$ is *R*3*c*, in agreement with the reported experimental low-temperature structure.[8] The reported and as-calculated *R*3*c* structures are compared in Supporting Information Table S1, with good agreement. Interestingly, although Table 1 shows that the octahedral rotation instabilities (M_3^+ and R_4^+) are

DOI: 10.1021/acs.inorgchem.5b01213
Inorg. Chem. 2015, 54, 8536−8543

present in both materials, $CsPbF_3$ adopts a structure with the $a^-a^-a^-$ tilt pattern, which is associated with R_4^+ only. As Figure 2 shows, *R*3*c* and *Pnma* structures are in close energetic

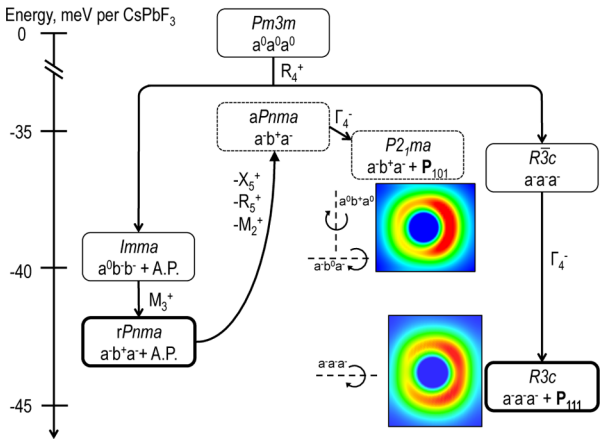

Figure 2. Stabilization per $CsPbF_3$ stoichiometric unit of structures with the $a^-b^+a^-$ and $a^-a^-a^-$ rotation patterns by polar and antipolar A-site displacements. Electron density maps are of the band corresponding to the σ^* orbital, spatially projected about the Pb^{2+} cation and cut in cross-section. Red corresponds to areas of greatest electron density. "A.P." denotes any and all antipolar displacement patterns that are commensurate with the space group produced by a given rotation pattern. Bold outlines indicate dynamically stable structures, thin solid outlines metastable structures, and dashed lines "frozen" structures that are not stable under internal relaxations. For both electron density maps, the polar mode is frozen in at an amplitude of 0.06*a* per formula unit, where *a* is the $Pm\bar{3}m$ lattice constant. All irreps are with respect to a $Pm\bar{3}m$ basis.

competition in $CsPbF_3$, as is the case in many oxide perovskites. How does the lone pair mediate the competition among different octahedral rotation patterns and between polar and nonpolar structures to make *R*3*c* the ground state of $CsPbF_3$? Why does the (polar) ground state of $CsPbF_3$ exhibit the $a^-a^-a^-$ rotation pattern rather than the much more common $a^-b^+a^-$?

Lone Pair Stereoactivity Is Not Sensitive to Octahedral Rotation Pattern. Since the ferroelectricity of $CsPbF_3$ appears to be driven by the stereoactivity of the Pb^{2+} lone pair, we compare the lone pair stereoactivity in structures with the $a^-a^-a^-$ and $a^-b^+a^-$ rotation patterns. We define *stereoactivity* as the chemical tendency (described below) of a lone pair cation to undergo an inversion-breaking distortion (lone pair localization), while *lone pair-driven ferroelectricity* describes whether such a distortion is energetically favorable.

The stereoactivity of the Pb^{2+} lone pair is the result of mixing of the formally empty Pb 6p orbital with the Pb 6s−F 2p σ^* orbital.[34,35] Such mixing requires both spatial overlap and energetic proximity between the Pb 6p and the σ^* orbitals. The Pb 6p and 6s orbitals are both localized about the Pb^{2+} cation; thus, the degree of spatial overlap between the Pb 6p and the σ^* orbitals is dependent upon the amount of Pb 6s character in the σ^* orbital. The σ^* orbital sits at the top of the valence band of $CsPbF_3$, while the bottom of the conduction band is primarily Pb 6p. Thus, the energetic proximity between these orbitals is described by the bandgap. Octahedral rotation patterns or other distortions that increase the Pb 6s character in the σ^* orbital and decrease the bandgap would enhance lone pair stereoactivity.

While only the R_4^+ and M_3^+ octahedral rotation modes are necessary to establish the *Pnma* symmetry, three other secondary modes are allowed by that symmetry as well. The X_5^+ mode, corresponding to antipolar A-site motion, is one such mode and the one that in oxide perovskites is typically the largest in magnitude after the R_4^+ and M_3^+ modes.[36] Because of the known role of the X_5^+ mode in suppressing the ferroelectric instability in *Pnma* perovskites,[36] we consider both the fully relaxed *Pnma* structure and *Pnma* with antipolar displacements manually removed.[37] We refer to this artificially constructed structure as a*Pnma*, in which the "a" stands for "antipolar displacement-free," and the fully relaxed structure as r*Pnma*.

We examine the densities of states of $CsPbF_3$ in the $R\bar{3}c$, a*Pnma*, and r*Pnma* structures to determine how their different octahedral rotation patterns and antipolar displacements affect the lone pair stereoactivity and find no qualitative differences (see Figure S2, Supporting Information). In particular, among these three structures there is no qualitative difference in the amount of Pb 6s character in the σ^* orbital, indicating comparable Pb 6p−σ^* spatial overlap; nor is there a qualitative difference in the bandgap, indicating comparable Pb 6p−σ^* energetic proximity. Hence, the chemical stereoactivity of the Pb^{2+} lone pair is not sensitive to the octahedral rotation pattern or to antipolar displacements in these nonpolar space groups.

A-Site Coordination Can Be Optimized by Polar Displacements in Structures with *R*$\bar{3}$*c* but Not *Pnma* Symmetry. Although the ferroelectricity in $CsPbF_3$ is driven by the Pb^{2+} lone pair, the Cs^+ cation plays a significant role in the crystal chemistry of this compound. As Table 2 shows, Cs

Table 2. Normalized Decomposition of the Softest Polar Force Constant Matrix Eigenmode of Various $CsPbF_3$ Structures[a]

	$Pm\bar{3}m$	$R\bar{3}c$	a*Pnma*	r*Pnma*
Cs	0.4103	0.2366	0.4851	0.1414
Pb	0.1381	0.1296	0.2763	0.0296
$F_{\parallel}$	0.3592	0.3781	0.5564	0.310
$F_{\perp}$	−0.5846	−0.6262	−0.4352	−0.6644

[a]Anionic displacements are labeled as either parallel ($F_{\parallel}$) or perpendicular ($F_{\perp}$) to the Pb−F bond.

makes a larger contribution than Pb to the ferroelectric eigenvector of $Pm\bar{3}m$, a*Pnma*, r*Pnma*, and $R\bar{3}c$ $CsPbF_3$. What role does the Cs^+ cation play in the ferroelectricity of $CsPbF_3$ and in determining the octahedral rotation pattern?

To test whether the antipolar displacements present in r*Pnma* are responsible for suppressing ferroelectricity in this structure, we calculated the frequency of the polar modes in a*Pnma*. In agreement with the results of Benedek and Fennie,[36] removing antipolar displacements does restore ferroelectricity, but the frequency of the polar mode in a*Pnma* ($i17$ cm^{-1}) is much harder than that in $R\bar{3}c$ ($i58$ cm^{-1}). Both polar modes, however, are associated with lone pair localization: a localized Pb^{2+} lone pair is visible in the electron densities of polar subgroups of both $R\bar{3}c$ and a*Pnma* (shown in Figure 2).

Figure 2 further shows that if we freeze in the polar eigenmode of a*Pnma* to form a structure of space group $P2_1ma$ (no. 26), the structure is stabilized by only 1.0 meV. This is substantially less than the amount that $R\bar{3}c$ is stabilized by its own polar mode (8.0 meV) and also less than the energy difference between r*Pnma* and fully relaxed *R*3*c* (1.6 meV). Even if the antipolar displacements of r*Pnma* had no effect on

DOI: 10.1021/acs.inorgchem.5b01213
Inorg. Chem. 2015, 54, 8536−8543

its ferroelectricity, $R3c$ would still be lower in energy than a polar subgroup of *Pnma*. Hence, the hardening effect of A-site antipolar displacements is not sufficient to explain why the ground state of $CsPbF_3$ is a polar subgroup of $R\bar{3}c$ rather than of *Pnma*. As we will see, however, A-site coordination preferences do play an important role both in the ferroelectricity of $CsPbF_3$ and in determining its ground state octahedral rotation pattern.

We use the bond valence model[38,39] to explore the Cs coordination in various structures. Brese and O'Keeffe[19] give a bond valence parameter, R_{Cs-F}, of 2.33 ± 0.02 Å for a Cs−F bond. This is an empirical value calculated through averaging over many structures. Because fully relaxed *Pnma* optimizes the A-site cation environment, we use it as a guide to adjust R_{Cs-F} for $CsPbF_3$ such that Cs in r*Pnma* has a bond valence sum of +1.000, its nominal value. We find that an appropriate value of R_{Cs-F} is 2.3505 Å.

By tracking changes to the Cs bond valence sum as the softest polar modes of $R\bar{3}c$, a*Pnma*, and r*Pnma* are frozen in at increasing magnitude, we compare how well a polar mode optimizes the A-site coordination environment in these different space groups. Figure 3 shows that for all structures

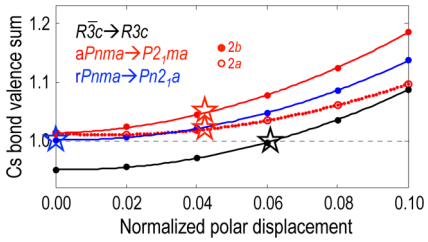

Figure 3. Cs bond valence sum for subgroups of $CsPbF_3$ calculated using our modified R_{Cs-F} value of 2.3505 Å. Use of Brese's R_{Cs-F} of 2.33 instead would cause a nearly static shift to slightly lower values (0.898 for nonpolar $R\bar{3}c$, 0.946 for nonpolar r*Pnma*, 0.956 for nonpolar a*Pnma*). The polar subgroup of a*Pnma*, $P2_1ma$, has two inequivalent Cs^+ cations, whose bond valences are plotted individually and which are labeled by Wyckoff position in $P2_1ma$; all other nonpolar parent structures and polar subgroups have just one unique Cs^+ site. Stars indicate the frozen polar structure with the lowest energy for each subgroup. Polar displacement magnitudes are given with respect to the lattice constant of $Pm\bar{3}m$ per formula unit. Curves are to guide the eye. The polar subgroup of the r*Pnma* structure is $Pn2_1a$, no. 33.

considered, the polar mode increases the Cs bond valence sum. The polar mode of $R\bar{3}c$ brings the Cs bond valence sum closer to unity. However, the bond valence sums of nonpolar r*Pnma* and a*Pnma* are already at or above unity, and the increase results in overcoordination of the A-site cation. While by our definition and construction the Cs coordination of r*Pnma* cannot be improved by any distortion, the same cannot be said for that in a*Pnma*. The X_5^+ and other antipolar modes found in r*Pnma* move the Cs^+ cations to improve their coordination. Why can the antipolar modes improve the Cs bond valence sum of a*Pnma*, but a polar mode does not?

Woodward[10] describes in detail the crystal chemistry of the antipolar cationic displacements that stabilize the A-site cation coordination environment in *Pnma*. As octahedral rotations become large, the bonds between the A-site cation and its three anionic nearest neighbors become too short. To lengthen these bonds and stabilize the structure, the A-site cation shifts away from them, along the black vector shown in Figure 4a (reproduced with permission from Woodward[10]). The spatial arrangement of the CsF_3 units in a*Pnma* $CsPbF_3$, as well as the three shortest Cs−F bond lengths, is shown in Figure 4b.

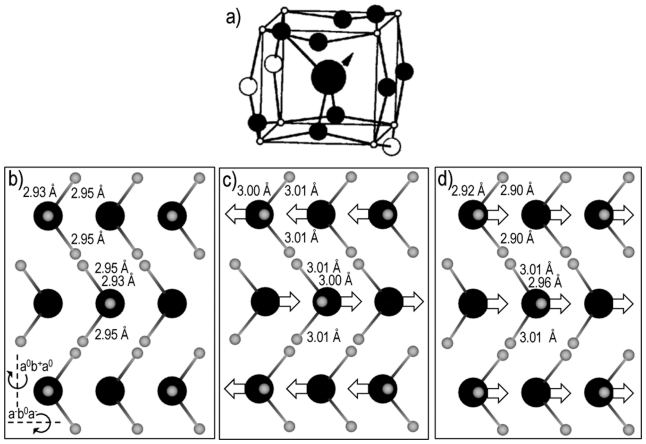

Figure 4. A-site coordination environments in $CsPbF_3$. Cs^+ or the A-site cations are shown as large black spheres throughout. In parts b−d, the F^- are shown as light gray spheres, and polar or antipolar displacements taken by the Cs^+ cations relative to the anion sublattice are shown as white arrows. Bond lengths are given for the three shortest Cs−F bonds. (a) The A-site cation and the bonds to its three nearest neighbor anions in a structure with *Pnma* symmetry, with the optimal cationic displacement vector shown as a black arrow. Reproduced from Woodward[10] with permission of the International Union of Crystallography: http://dx.doi.org/10.1107/S0108768196012050. (b) The CsF_3 units of a*Pnma* $CsPbF_3$. (c) The CsF_3 units of r*Pnma* $CsPbF_3$. (d) The CsF_3 units of a*Pnma* $CsPbF_3$ with its softest polar phonon mode frozen in giving space group $P2_1ma$.

Due to the symmetry of space group *Pnma*, each CsF_3 polyhedron is inverted relative to its neighbors along the pseudocubic [010] axis (the axis about which the in-phase octahedral rotations have occurred), inverting these displacement vectors as well. The resulting globally antipolar displacement pattern optimizes the bonding environment of all A-site cations in the crystal simultaneously, as shown in Figure 4c. A globally polar (ferroelectric) displacement pattern, on the other hand, breaks the symmetry of the CsF_3 units. Figure 4d shows the change to the CsF_3 units and the Cs−F bond lengths when the softest polar mode of a*Pnma* is frozen in, to give a structure of space group $P2_1ma$, along with the displacement vectors taken by each Cs^+ cation. In half of the CsF_3 units of $P2_1ma$ the Cs−F bonds are longer than those in a*Pnma*; in the other CsF_3 units of $P2_1ma$ the Cs−F bonds have been *shortened*! Because the Cs displacements are driven by the need to lengthen the bonds of the CsF_3 units, it is easy to see why such a polar displacement pattern is less favorable than the antipolar one.

We now turn from space group *Pnma* to $R\bar{3}c$. Unlike in a*Pnma*, the A-site of $R\bar{3}c$ is undercoordinated, not overcoordinated (as seen in Figure 3). The A-site cation of $R\bar{3}c$ sits in a 3 + 6 coordinate environment, with the three short bonds coplanar with the A cation. The displacements that transform $R\bar{3}c$ to $R3c$ lengthen the three shortest A−X bonds while shortening three of the other six by moving the A cation along the pseudocubic [111] axis (the axis about which the octahedra have rotated).[36] Based on the site symmetry of the A-site in $R\bar{3}c$, displacements of a given A-site cation in either the [111] direction or the antiparallel $[\bar{1}\bar{1}\bar{1}]$ direction are equivalent by

DOI: 10.1021/acs.inorgchem.5b01213
Inorg. Chem. 2015, 54, 8536−8543

symmetry. Thus, moving the A-site cations in a globally parallel pattern has the same effect on their local environments as moving them in an antiparallel one. As a result of $R\bar{3}c$ symmetry, *unlike in Pnma, displacing all A-site cations of* $R\bar{3}c$ *in parallel can optimize all the A-site coordination environments simultaneously.*

Our findings are consistent with previous work regarding the stabilization of polar subgroups of *Pnma* perovskites using biaxial tensile strain. In both $CaTiO_3$[40] and $CaMnO_3$,[41] +2% biaxial strain in the pseudocubic (010) plane (normal to the M_3^+ rotation axis) softens polar phonon modes of *Pnma* and stabilizes a polar subgroup. For both compounds, the stabilized polarization vector lies in the (010) plane; in $CaTiO_3$ polarization in the pseudocubic $[10\bar{1}]$ direction (resulting in subgroup $Pnm2_1$, no. 31) is slightly more favorable than in the [101] (resulting in subgroup $P2_1ma$, the same as the polar subgroup of a*Pnma* $CsPbF_3$), though structures with polarization in either direction are dynamically stable. Bhattacharjee and co-workers[41] comment that tensile strain "provides more space for the ferroelectric distortion", in concord with our finding that overcoordination of the A-site cation by polar distortions is responsible for the disfavoring of polar instabilities in *Pnma*.

Anionic Displacements Mediate the Interaction between B-Site Lone Pair-Driven Ferroelectricity and A-Site Coordination Environment. We now address how the A-site bonding preferences, which disfavor polar phonon instabilities, suppress the B-site lone pair-driven ferroelectricity in *Pnma* $CsPbF_3$. Historically, ferroelectric distortions in perovskites have been described as polar displacements of the cations against rigid anion octahedra.[42] However, it is now appreciated that distortions of the anion octahedra, in addition to cationic displacements, are important.[43−45]

We refer back to Table 2 for the contribution of anionic displacements to the polar force constant matrix eigenvectors of $CsPbF_3$ in structures with $R\bar{3}c$ and *Pnma* symmetry, the latter both with and without antipolar displacements. In all three structures, the anionic displacements are large. As seen in the inset of Figure 5, the polar eigenvectors of these structures distort the PbF_6 octahedra substantially, which will have the effect of changing not just the B-site environment but the A-site one as well.

We compare in Figure 5 how the energy of $R\bar{3}c$, a*Pnma*, and r*Pnma* evolves when freezing in to each structure its complete softest polar eigenvector to how the energy evolves when the anionic displacements are suppressed. We give the displacement magnitude of the complete eigenvector with respect to the $Pm\bar{3}m$ lattice constant per formula unit. Freezing in the complete eigenvectors of $R\bar{3}c$ and a*Pnma* lowers the energy of both structures. However, when anionic displacements are suppressed, the energy of both structures instead increases monotonically. (The softest polar eigenvector of r*Pnma* has a positive force constant, so even the complete eigenvector increases the energy when frozen in.)

As shown in Figure S4 (see Supporting Information), anionic displacements increase the mixing of the Pb 6p with the Pb 6s−F 2p σ^* orbital and thus lone pair stereoactivity. Furthermore, structures in the polar subgroups of $R\bar{3}c$, a*Pnma*, and r*Pnma* all exhibit more Pb s in the conduction band and more Pb p in the valence band when the anionic displacements are present. Hence, the stereoactivity of the lone pair is sensitive to the anionic displacements that accompany the polar distortion. This is in contrast to its insensitivity, shown earlier, to the anionic displacements that characterize the octahedral rotation patterns of nonpolar $R\bar{3}c$, a*Pnma*, and r*Pnma*. *Anionic displacements, which modify both the A- and the B-site environments, are essential to lone pair-driven ferroelectricity in* $CsPbF_3$.

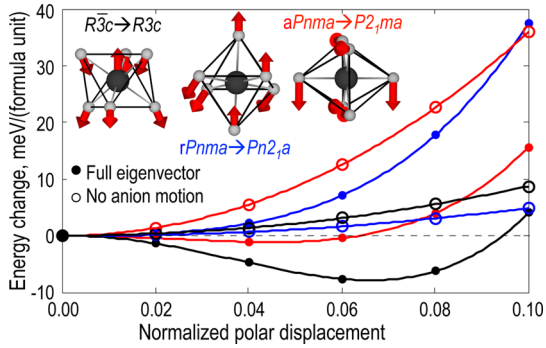

Figure 5. Dependance of changes in the total energy per formula unit on increasing polar displacement amplitude. Polar structures with F motion are made by freezing in the softest polar force constant matrix eigenvector of the relevant structure at the given magnitude times the $Pm\bar{3}m$ lattice constant per formula unit. Polar structures without F motion are made in the same way but with the anionic displacements from the nonpolar structure set to zero. Displacement vectors are not renormalized after F motion is removed. Lines between points serve as a guide for the eye. Results are qualitatively the same for polar distortions of $Pm\bar{3}m$ (see Supporting Information Figure S3). Inset: manner in which the softest polar force constant matrix eigenvectors distort the PbF_6 octahedra. Octahedra are oriented such that motion of the Cs^+ cations (not shown) is toward the top of the page.

Lone Pair Localizing Modes Favor Polar Rather than Antipolar Displacement Patterns. Localization of the Pb^{2+} lone pair requires breaking local inversion symmetry about the B-site. This may occur as part of a global displacement pattern that is either polar or antipolar in nature. Corner connectivity of the PbF_6 octahedra dictates that as the octahedra distort with an inversion-breaking distortion in space group *R*3*c*, all B-site displacements will occur in parallel rather than in antiparallel.[46] As we show below, the same requirement of connectivity of the BX_6 octahedra also requires parallel rather than antiparallel B-site displacements along the pseudocubic [101] direction, the direction of the softest polar mode of a*Pnma* as well as of the antipolar displacements found in r*Pnma*. Thus, the structural preference for antipolar A-site displacements resulting from the $a^-b^+a^-$ rotation pattern are in direct competition with the B-site-driven ferroelectricity.

The most pronounced structural change to the PbF_6 octahedra when distorted by the polar mode of a*Pnma*, as seen in the inset to Figure 5, is the elongation of one F−F edge and the shortening of the opposite edge. Figure 6a gives a simplified picture of how such a polar mode changes these F−F bond lengths, using a $Pm\bar{3}m$ parent structure for visual clarity. The resulting octahedral shapes, greatly exaggerated to emphasize the effects of these distortions, is shown in Figure 6b, as well as the orientation of the Pb^{2+} lone pairs that would localize as a result of such a distortion.

As we showed in the previous section, these anionic displacements are necessary for stabilization of polar structures and substantially enhance the orbital mixing associated with lone pair stereoactivity. The octahedral distortion pattern schematized in Figure 6 results in a polar arrangement of localized Pb^{2+} lone pairs. To flip half of the Pb^{2+} lone pair orientations and create a globally antipolar lone pair pattern,

DOI: 10.1021/acs.inorgchem.5b01213
Inorg. Chem. 2015, 54, 8536−8543

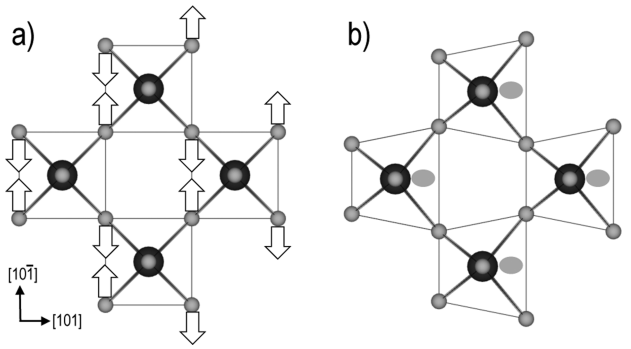

Figure 6. A schematic representation of (a) how polarization along the [101] direction would move the F^- anions in $Pm\bar{3}m$ and (b) the resulting distortions of the PbF_6 octahedra. For visual clarity, no octahedral rotations are present, F^- anions are only moved along the [101$^-$] direction, Pb^{2+} cations are not moved at all, and Cs^+ cations are not shown. Pb^{2+} are represented as large, black spheres, F^- as small, light gray spheres, Pb−F bonds as thick rods, F−F edges as thin lines, and localized Pb^{2+} lone pairs as pale gray ovals.

the local Pb^{2+} coordination environments, that is, the associated PbF_6 octahedra, would have to be flipped as well. Such an arrangement would destroy the corner connectivity of the PbF_6 octahedra. Thus, not only to do anionic displacements mediate the interaction between the B-site lone pair driven ferroelectricity of $CsPbF_3$ and the octahedral rotation pattern, but they also account for the polar, rather than antipolar, arrangement of the localized Pb^{2+} lone pairs in the ground state of $CsPbF_3$.

Implications for Inorganic ABX_3 Ferroelectrics, Oxide Perovskites, and Hybrid Perovskite Photovoltaics. The Pb^{2+} lone pair cation stabilizes the ferroelectric ground state of $CsPbF_3$, just as A-site lone pair cations may stabilize ferroelectric ground states in oxide perovskites. We showed in the previous section that B-site lone pair cations will prefer to localize in a parallel arrangement, resulting in a global polarization. We therefore recommend the investigation of other ABX_3 compounds with B = Ge, Sn, and Pb as potential ferroelectrics.

While $CsPbF_3$ is the only experimentally verified polar ABF_3 perovskite that we were able to locate in the literature, there are a few other polar ABX_3 perovskites with monatomic, nonmolecular A^+ and B^{2+} cations and X, a halide. Thiele and colleagues[47] report that $CsGeX_3$ (X = Cl, Br, or I; t = 1.03, 1.01, or 0.99)[48] all exist experimentally as $R3m$ perovskites at room temperature, with a polarization along the [111] direction with respect to the cubic perovskite unit cell. $APbI_3$ (A = Cs, Rb;[49] t = 0.91, 0.87) and $CsSnX_3$ (X = Cl, Br, I;[50] t = 0.95, 0.93, 0.92) are computationally predicted to exhibit relatively high high-frequency dielectric constants and, in the case of $CsSnI_3$, imaginary-frequency polar modes,[51] when constrained to the $Pm\bar{3}m$ perovskite structure. However, only $CsSnBr_3$[52] and possibly $CsSnI_3$[53] are experimentally stable in the perovskite structure at room temperature, and both are reported to form in nonpolar structures. $CsPbI_3$,[54] $RbPbI_3$,[54] and $CsSnCl_3$[55] are reported to form in non-perovskite phases at room temperature. $CsPbCl_3$ (t = 0.89) is experimentally reported to form as a nonpolar perovskite with octahedral rotations.[56] $RbPbF_3$ (t = 0.89) is experimentally reported to form a non-perovskite structure at room temperature and undergo a phase transition to the $Pm\bar{3}m$ perovskite structure at high temperature.[57]

As evidenced by the variety of both polar and nonpolar phases reported in the literature, the simple presence of Ge^{2+}, Sn^{2+}, or Pb^{2+} is insufficient to guarantee a ferroelectric perovskite ground state.[58] The stereoactivity of a lone pair cation depends not just on the cation itself but also on the anions to which it is bonded,[34] as well as their interatomic spacing (bond length). Substitution of different halide anions may be used to tune the stereoactivity of a lone pair cation by changing the energetic proximity of the relevant orbitals;[35] substitution of larger or smaller A-site cations may be used to change the spatial overlap between those orbitals and further tune the lone pair stereoactivity, especially when tolerance factor is near or above unity and octahedral rotations are suppressed. In the non-perovskite ground state structures of $CsPbI_3$, $CsSnCl_3$, $RbPbI_3$, and $RbPbF_3$, the lone pair B^{2+} cation sits at a site with broken inversion symmetry, meaning that the lone pair may be active; in $CsSnCl_3$ and $RbPbF_3$, the B cations are also highly off-center within their coordination polyhedra. It should be considered whether the B cation lone pairs in these latter two compounds are so highly stereoactive and favor such strongly distorted environments that the perovskite structure is destabilized.

Turning now to the applicability of our results for $CsPbF_3$ to the oxide perovskites, the reason for the weakening of ferroelectric instabilities by the $a^-b^+a^-$ rotation pattern does not depend on the presence of a B-site lone pair cation or on the particular chemical nature of the anion. This reasoning is therefore transferable to the oxides, though we note that $Pnma$ has more than one polar subgroup, and our discussion has focused on just one of them, $P2_1ma$.

The transferability will be poorer from our findings regarding the effect of lone pair cations on the B-site to the effect of lone pair cations on the A-site. While we have argued that localized B-site lone pair cations will prefer to orient in parallel, the equivalent statement cannot be made for localized A-site lone pairs: while the localized lone pairs of $PbTiO_3$ and $BiFeO_3$ orient in parallel, those of $PbZrO_3$ are oriented in an antiparallel fashion. How anionic displacements couple to the localization of A-site lone pairs is beyond the scope of this work but is apparently in a manner distinct from their coupling to the localization of B-site lone pairs.

We last turn to the organic−inorganic hybrid ABX_3 perovskite solar cell materials. Small organic molecules, prototypically $CH_3NH_3^+$, sit on the A site; a divalent lone pair cation, nearly always Pb^{2+} but occasionally Sn^{2+}, sits on the B site; and heavy halides I^-, Br^-, or Cl^- sit on the X sites.[7] It is still not fully understood whether the Pb^{2+} lone pairs are localized in these compounds at room temperature or what the role of such localization would be on device performance.[7] A number of hybrid perovskite materials[59−61] with Pb^{2+} or Sn^{2+} on the B-site do form in polar structures or even exhibit ferroelectricity; however, as of yet studies have focused upon the role of the organic molecules in these phenomena[60,61] not the cationic lone pair. The high dielectric constant of prototypical hybrid perovskite photovoltaic $(CH_3NH_3)PbI_3$ has been identified as an important contributor to its high efficiency.[60] Because the dielectric constant of a material will diverge as a proper ferroelectric transition is approached,[62] we suggest tuning lone pair stereoactivity to approach a lone pair driven ferroelectric transition as a means to further improve these already very successful materials.

We apply our design rules for tuning lone pair stereoactivity to the hybrid $APbX_3$ perovskites, using $(CH_3NH_3)PbI_3$ as an example. If we approximate the A-site cation as a sphere, increasing its size in the absence of octahedral rotations will

DOI: 10.1021/acs.inorgchem.5b01213
Inorg. Chem. 2015, 54, 8536−8543

lengthen the Pb−X bonds and decrease lone pair stereoactivity. On the other hand, using smaller halides (Br^- or Cl^-) would increase lone pair stereoactivity both by favoring shorter Pb−X bonds and by increasing the energetic proximity of the relevant Pb and X orbitals.[35] While the efficiency of a photovoltaic device depends on many factors that we have not treated here, we believe that tuning the lone pair stereoactivity in this way has the potential to increase device performance.

CONCLUSIONS

We have used first-principles calculations to study the origin of ferroelectricity in the only ABF_3 compound that has been experimentally shown to exist as a perovskite with a polar ground state. Because the lone pair free analogue of $CsPbF_3$, $CsSrF_3$, lacks a polar instability, we attribute the ferroelectricity of $CsPbF_3$ to the Pb^{2+} lone pair.

We find that the polar ground state of $CsPbF_3$, space group *R*3*c*, is in close energetic competition with a nonpolar structure of space group *Pnma*, which lacks a polar instability. Even in the absence of antipolar displacements, the $a^-b^+a^-$ rotation pattern weakens ferroelectric instabilities relative to the $a^-a^-a^-$. There are no qualitative differences in the Pb s- and Pb p-projected densities of states among $R\bar{3}c$, fully relaxed *Pnma*, and *Pnma* with antipolar displacements removed, indicating comparable chemical stereoactivity of the Pb^{2+} cation in the three structures.

While without its lone pair cation $CsPbF_3$ would not be ferroelectric, we find that there is also a significant A-site contribution to the ferroelectric eigenmode. *Pnma* symmetry prevents the ferroelectric eigenmode of $CsPbF_3$ from optimally coordinating all A-site cations of structures in this space group at once. This is not true in space group $R\bar{3}c$: $R\bar{3}c$ symmetry allows a globally polar displacement pattern to simultaneously satisfy the coordination requirements of all A-site cations.

The localization of the Pb^{2+} lone pair requires a polar pattern of anionic displacements, placing lone pair localization and A-site optimization in direct competition when rotation pattern $a^-b^+a^-$ is present but not when $a^-a^-a^-$ is present instead. The ground state of $CsPbF_3$ has space group *R*3*c* because in that space group the combination of octahedral rotations and ferroelectricity simultaneously satisfy the A-site bonding requirements and allow the Pb^{2+} lone pair to localize.

ASSOCIATED CONTENT

Supporting Information

The Supporting Information is available free of charge on the ACS Publications website at DOI: 10.1021/acs.inorgchem.5b01213.

Version and potential information for computational software, phonon band structures and densities of states of $CsPbF_3$ and $CsSrF_3$, comparison of experimental and theoretical *R*3*c* $CsPbF_3$ structures, electronic densities of states of polar and nonpolar $CsPbF_3$ structures, energetic stabilization associated with the polar mode of $Pm\bar{3}m$ $CsPbF_3$ with and without anionic displacements, and coordinates of relaxed structures from first-principles calculations (PDF)

AUTHOR INFORMATION

Corresponding Authors

*E-mail: ehs73@cornell.edu (E.H.S.).
*E-mail: nicole.benedek@austin.utexas.edu (N.A.B.).

Notes

The authors declare no competing financial interest.

ACKNOWLEDGMENTS

E.H.S. and C.J.F. were supported by the DOE-BES under Award No. DE-SC0005032. N.A.B. was supported by The Welch Foundation under Grant No. F-1803. The authors thank P. Shiv Halasyamani, Ram Seshadri, Pat Woodward, and Young-Moo Byun for useful discussions.

REFERENCES

(1) Goldschmidt, V. M. *Naturwissenschaften* **1926**, *14*, 477−485.
(2) Babel, D.; Tressaud, A. Crystal Chemistry of Fluorides. In *Inorganic Solid Fluorides: Chemistry and Physics*; Hagenmuller, P., Ed.; Academic Press, Inc.: Orlando, FL, 1985; Chapter 3.
(3) FIZ Karlsruhe, International Crystal Structure Database. icsd.fiz-karlsruhe.de/icsd, 2013.
(4) SpringerMaterials - The Landolt-Börnstein Database. www.springermaterials.com, 2014.
(5) Kojima, A.; Teshima, K.; Shirai, Y.; Miyasaka, T. J. *J. Am. Chem. Soc.* **2009**, *131*, 6050−6051.
(6) Lee, M. M.; Teuscher, J.; Miyasaka, T.; Murakami, T. N.; Snaith, H. J. *Science* **2012**, *338*, 643−7.
(7) Green, M. A.; Ho-Baillie, A.; Snaith, H. J. *Nat. Photonics* **2014**, *8*, 506−514.
(8) Berastegui, P.; Hull, S.; Eriksson, S.-G. *J. Phys.: Condens. Matter* **2001**, *13*, 5077−5088.
(9) Glazer, A. M. *Acta Crystallogr., Sect. B: Struct. Crystallogr. Cryst. Chem.* **1972**, *B28*, 3384−3392.
(10) Woodward, P. M. *Acta Crystallogr., Sect. B: Struct. Sci.* **1997**, *B53*, 44−66.
(11) Thomas, N. W. *Acta Crystallogr., Sect. B: Struct. Sci.* **1996**, *B52*, 16−31.
(12) Garcia-Castro, A. C.; Spaldin, N. A.; Romero, A. H.; Bousquet, E. *Phys. Rev. B: Condens. Matter Mater. Phys.* **2014**, *89*, 104107.
(13) Perdew, J. P.; Ruzsinszky, A.; Csonka, G. I.; Vydrov, O. A.; Scuseria, G. E.; Constantin, L. A.; Zhou, X.; Burke, K. *Phys. Rev. Lett.* **2008**, *100*, 136406.
(14) Kresse, G.; Hafner, J. *Phys. Rev. B: Condens. Matter Mater. Phys.* **1993**, *47*, 558−561.
(15) Kresse, G.; Furthmüller, J. *Phys. Rev. B: Condens. Matter Mater. Phys.* **1996**, *54*, 11169−11186.
(16) Baroni, S.; Resta, R. *Phys. Rev. B: Condens. Matter Mater. Phys.* **1986**, *33*, 7017−7021.
(17) Gajdos, M.; Hummer, K.; Kresse, G.; Furthmüller, J.; Bechstedt, F. *Phys. Rev. B: Condens. Matter Mater. Phys.* **2006**, *73*, 045112.
(18) Kresse, G.; Joubert, D. *Phys. Rev. B: Condens. Matter Mater. Phys.* **1999**, *59*, 1758−1775.
(19) Brese, N. E.; O'Keeffe, M. *Acta Crystallogr., Sect. B: Struct. Sci.* **1991**, *B47*, 192−197.
(20) Stokes, H. T.; Hatch, D. M.; Campbell, B. J. ISOTROPY software suite. stokes.byu.edu/iso/isotropy.php, 2014.
(21) Aroyo, M. I.; Perez-Mato, J. M.; Orobengoa, D.; Tasci, E.; de la Flor, G.; Kirov, A. *Bulg. Chem. Commun.* **2011**, *43*, 183−197.
(22) Aroyo, M. I.; Perez-Mato, J. M.; Capillas, C.; Kroumova, E.; Ivantchev, S.; Gadariaga, G.; Kirov, A.; Wondratschek, H. *Z. Kristallogr.* **2006**, *221*, 15−27.
(23) Aroyo, M. I.; Kirov, A.; Capillas, C.; Perez-Mato, J. M.; Wondratschek, H. *Acta Crystallogr., Sect. A: Found. Crystallogr.* **2006**, *A62*, 115−128.
(24) Orobengoa, D.; Capillas, C.; Aroyo, M. I.; Perez-Mato, J. M. *J. Appl. Crystallogr.* **2009**, *42*, 820−833.
(25) Perez-Mato, J. M.; Orobengoa, D.; Aroyo, M. I. *Acta Crystallogr., Sect. A: Found. Crystallogr.* **2010**, *A66*, 558−90.
(26) Mostofi, A. A.; Yates, J. R.; Lee, Y.-S.; Souza, I.; Vanderbilt, D.; Marzari, N. *Comput. Phys. Commun.* **2008**, *178*, 685−699.
(27) Korytar, R.; Pruneda, M.; Junquera, J.; Ordejon, P.; Lorente, N. *J. Phys.: Condens. Matter* **2010**, *22*, 385601.

DOI: 10.1021/acs.inorgchem.5b01213
Inorg. Chem. 2015, 54, 8536−8543

(28) Momma, K.; Izumi, F. *J. Appl. Crystallogr.* **2011**, *44*, 1272−1276.
(29) Togo, A.; Oba, F.; Tanaka, I. *Phys. Rev. B: Condens. Matter Mater. Phys.* **2008**, *78*, 134106.
(30) Roth, W. L.; Devries, R. C. *J. Appl. Phys.* **1967**, *38*, 951−952.
(31) Belik, A. A.; Iikubo, S.; Kodama, K.; Igawa, N.; Shamoto, S.-i.; Maie, M.; Nagai, T.; Matsui, Y.; Stefanovich, S. Y.; Lazoryak, B. I.; Takayama-Muromachi, E. *J. Am. Chem. Soc.* **2006**, *128*, 706−707.
(32) Belik, A. A.; Wuernisha, T.; Kamiyama, T.; Mori, K.; Maie, M.; Nagai, T.; Matsui, Y.; Takayama-Muromachi, E. *Chem. Mater.* **2006**, *18*, 133−139.
(33) Lufaso, M. W.; Woodward, P. M. *Acta Crystallogr., Sect. B: Struct. Sci.* **2001**, *B57*, 725.
(34) Waghmare, U.; Spaldin, N.; Kandpal, H.; Seshadri, R. *Phys. Rev. B: Condens. Matter Mater. Phys.* **2003**, *67*, 125111.
(35) Walsh, A.; Payne, D. J.; Egdell, R. G.; Watson, G. W. *Chem. Soc. Rev.* **2011**, *40*, 4455−63.
(36) Benedek, N. A.; Fennie, C. J. *J. Phys. Chem. C* **2013**, *117*, 13339−13349.
(37) In addition to the X_5^+ mode, we also remove the M_2^+ and R_5^+, leaving only the octahedral rotations.
(38) Brown, I. D. *Chem. Soc. Rev.* **1978**, *7*, 359−376.
(39) Brown, I. D. *Chem. Rev.* **2009**, *109*, 6858−6919.
(40) Eklund, C.-J.; Fennie, C. J.; Rabe, K. M. *Phys. Rev. B: Condens. Matter Mater. Phys.* **2009**, *79*, 220101(R).
(41) Bhattacharjee, S.; Bousquet, E.; Ghosez, P. *Phys. Rev. Lett.* **2009**, *102*, 117602.
(42) Lines, M. E.; Glass, A. M. *Principles and Applications of Ferroelectrics and Related Materials*; Clarendon Press: Oxford, U.K, 2011.
(43) Ghosez, P.; Cockayne, E.; Waghmare, U. V.; Rabe, K. M. *Phys. Rev. B: Condens. Matter Mater. Phys.* **1999**, *60*, 836−843.
(44) Grinberg, I.; Rappe, A. M. *Phase Transitions* **2007**, *80*, 351−368.
(45) Lebedev, A. I. *Phys. Solid State* **2009**, *51*, 362−372.
(46) Thomas, N. W.; Beitollahi, A. *Acta Crystallogr., Sect. B: Struct. Sci.* **1994**, *B50*, 549−560.
(47) Thiele, G.; Rotter, H. W.; Schmidt, K. D. *Z. Anorg. Allg. Chem.* **1987**, *545*, 148−156.
(48) Bond valences for Ge^{2+} compounds were calculated using Shannon radii.
(49) Brgoch, J.; Lehner, A. J.; Chabinyc, M.; Seshadri, R. *J. Phys. Chem. C* **2014**, *118*, 27721−27727.
(50) Huang, L.-y.; Lambrecht, W. R. L. *Phys. Rev. B: Condens. Matter Mater. Phys.* **2013**, *88*, 165203.
(51) da Silva, E. L.; Skelton, J. M.; Parker, S. C.; Walsh, A. *Phys. Rev. B: Condens. Matter Mater. Phys.* **2015**, *91*, 144107.
(52) Mori, M.; Saito, H. *J. Phys. C: Solid State Phys.* **1986**, *19*, 2391−2401.
(53) Chung, I.; Song, J.-H.; Im, J.; Androulakis, J.; Malliakas, C. D.; Li, H.; Freeman, A. J.; Kenney, J. T.; Kanatzidis, M. G. *J. Am. Chem. Soc.* **2012**, *134*, 8579−8587.
(54) Trots, D. M.; Myagkota, S. V. *J. Phys. Chem. Solids* **2008**, *69*, 2520−2526.
(55) Poulsen, F. R.; Rasmussen, S. E.; et al. *Acta Chem. Scand.* **1970**, *24*, 150−156.
(56) Fujii, Y.; Hoshino, S.; Yamada, Y.; Shirane, G. *Phys. Rev. B* **1974**, *9*, 4549.
(57) Yamane, Y.; Yamada, K.; Inoue, K. *Solid State Ionics* **2008**, *179*, 483.
(58) Stoltzfus, M. W.; Woodward, P. M.; Seshadri, R.; Klepeis, J.-h.; Bursten, B. *Inorg. Chem.* **2007**, *46*, 3839−3850.
(59) Stoumpos, C. C.; Malliakas, C. D.; Kanatzidis, M. G. *Inorg. Chem.* **2013**, *52*, 9019−9038.
(60) Frost, J. M.; Butler, K. T.; Walsh, A. *APL Mater.* **2014**, *2*, 081506.
(61) Frost, J. M.; Butler, K. T.; Brivio, F.; Hendon, C. H.; van Schilfgaarde, M.; Walsh, A. *Nano Lett.* **2014**, *14*, 2584−2590.
(62) Rabe, K. M., Ahn, C. H., Triscone, J.-M., Eds. *Physics of Ferroelectrics: A Modern Perspective*; Topics in Applied Physics; Springer: Berlin, Germany, 2007; Vol. *105*.

DOI: 10.1021/acs.inorgchem.5b01213
Inorg. Chem. 2015, 54, 8536−8543